Title

Boosting photovoltaic performance of ternary organic solar cells by integrating a multi-functional guest acceptor



Authors

Yin, Yuli

Zhan, Lingling

Liu, Ming

et al.

Publication Date

2021-12-01

DOI

10.1016/j.nanoen.2021.106538

Peer reviewed

# Boosting photovoltaic performance of ternary organic solar cells by integrating a multi-functional guest acceptor

Yuli Yin [a,e,1], Lingling Zhan [c,1], Ming Liu [a], Chongqing Yang [b], Fengyun Guo [a], Yi Liu [b,*], Shiyong Gao [a], Liancheng Zhao [a], Hongzheng Chen [c,**], Yong Zhang [a,d,***]

[a] *School of Materials Science and Engineering, Harbin Institute of Technology, Harbin 150001, P. R. China*

[b] *The Molecular Foundry, Lawrence Berkeley National Laboratory, One Cyclotron Road, Berkeley, CA 94720, USA*

[c] *State Key Laboratory of Silicon Materials, MOE Key Laboratory of Macromolecular Synthesis and Functionalization, Department of Polymer Science and Engineering, Zhejiang University, Hangzhou 310027, P. R. China*

[d] *School of Materials Science and Engineering, Zhengzhou University, Zhengzhou 450001, P. R. China*

[e] *School of Chemistry and Chemical Engineering, University of South China, Hengyang 421001, P. R. China*

[*] Corresponding author.

[**] Corresponding author.

[***] Corresponding author.

*E-mail addresses:* yliu@lbl.gov (Y. Liu), hzchen@zju.edu.cn (H. Chen), yongzhang@hit.edu.cn (Y. Zhang).

[1] Yuli Yin and Lingling Zhan contributed equally to this work.

**Abstract**

Constructing ternary structure is one of the most effective design strategies to break the efficiency ceiling of traditional binary organic solar cells (OSCs). Here, a new Y-series non-fullerene acceptor (Y-T) featuring 1,3-diethyl-2-thiobarbituric acid (DTBA) end groups is developed as a third component for the classical PM6:Y6 binary system. The champion power conversion efficiency of ternary OSCs is increased from 15.64% to 17.37% via incorporating 10 wt% Y-T, with the simultaneously enhanced open-circuit voltage ($V_{oc}$) of 0.865 V, a short-circuit current density ($J_{sc}$) of 26.90 mA/cm$^2$, and a fill factor (FF) of 74.97%. The positive contribution of Y-T in the ternary blend can be ascribed to the improved spectroscopic complementarity and enhanced exciton utilization ratio due to the additional energy transfer process. Moreover, Y-T guest acceptor plays a critical role in adjusting the active layer morphology and facilitating three-dimension phase separation, resulting in a balanced charge transport and enhanced FF of ternary OSCs. This work provides insight into the molecular design of non-fullerene acceptor and suggest guidelines to rationally select guest component for ternary OSCs.

**Keywords:** Electron acceptor, Ternary organic solar cells, Energy transfer, Electronic alloy acceptors, 3D phase separation

## 1. Introduction

Non-fullerene acceptors (NFAs) have emerged as a crucial research endeavor that has significantly advanced the field of bulk-heterojunction organic solar cells (OSCs). Many state-of-the-art NFAs have been developed over the past few years [1-10]. Among these NFAs, the A-DA'D-A type Y6 acceptor with the feature of near-infrared light harvesting and high electron affinity has recently reached an outstanding power conversion efficiencies (PCEs) of over 16% when paired with polymer donors in binary OSCs [10-16]. The successful material design has appealed numerous efforts in modifying the core structure of Y6, such as altering the alkyl chains, halogen substitutes, extending conjugation length and changing the electron deficient unit of the Y6 core, etc., in aiming to further improve the PCEs of OSCs [17-23]. Another convenient and efficient strategy to advance the limit of photovoltaic performances of Y6-based OSCs is to introduce a third component into the binary system [24-28]. By introducing either a polymer donor or an electron acceptor as the third component, it can imbue the active layer with broadened absorption, balanced crystallinity, and improved film morphology, all conducive to a higher overall device performance [29-34]. For example, Hou et al. incorporated $PC_{61}BM$ as the third component to fabricate PM6:Y6:$PC_{61}BM$ ternary OSCs, which achieved a PCE of 16.50% due to the more balanced charge transport and reduced energy losses [35]. However, the limited absorption and energetic tunability of fullerene derivatives impose severe restrictions on further performance enhancement of the corresponding ternary OSCs. Regarding this limit, Yan et al. utilized an ultra-narrow bandgap NFA with a $E_g$ of 1.24 eV as the

third component to improve the short-circuit current density ($J_{sc}$) and thereby the PCE, but this ternary OSC exhibited a lower open circuit voltage ($V_{oc}$) and higher energy loss than that of the binary system due to the much lower lowest unoccupied molecular orbital (LUMO) energy level [36]. The demonstrated trade-off between $V_{oc}$ and $J_{sc}$ calls for a delicate design of the third component that can concurrently improve the relevant device characteristics in the ternary blend systems.

In the one polymer donor and two acceptors ternary system, the acceptor that play the primary role called host acceptor, while the guest acceptor serves as secondary role. Theoretically, if the guest acceptor has a higher-lying LUMO level than that of the host acceptor, the ternary OSC will be able to provide a higher $V_{oc}$ than the binary OSC [24, 29, 37]. Improving $J_{sc}$ is relatively more complicated since it concerns not only the absorption complementarity but more importantly, the morphology of the ternary blend because the materials' compatibility plays a deterministic role in influencing nanoscale phase separation in the active layer. One of the molecular design considerations for achieving favorable morphology in ternary systems is to retain similar backbone structures for both the guest and host acceptors, which is more preferable for the formation of well-mixed alloy states and beneficial for improving charge carrier separation, transport, and correspondingly $J_{sc}$ [38-42]. In addition, this similarity in the acceptors' chemical skeleton has also been shown to effectively reduce trap density in ternary OSCs [43]. In the state-of-the-art PM6:Y6 system, a few Y6 derivatives have been developed as the guest acceptor to achieve improved device performance [40-42]. These Y6-derived acceptors are currently

dominated by these employing the malononitrile-derived indanone (ICs) end groups. Small structural variations such as halogenation and methylation on the IC groups were incorporated, which resulted in minor changes of absorption spectra and energy levels. Despite good compatibility between the acceptors, their similar absorptivity in the ternary blend films may lead to the competition of absorbing sunlight. To further improve the photovoltaic performance in the ternary blend system, a desirable strategy is to design a guest acceptor with high-lying LUMO level and significantly shifted absorption with respect to the host acceptor (i.e. Y6) while retaining a similar core structure.

In this work, we design and synthesize a novel guest acceptor, Y-T, by employing the weakly electron-withdrawing 1,3-diethyl-2-thiobarbituric acid (DTBA) as the end group, which can fine-tune the aggregation behavior of Y-T and also provide significantly higher lying LUMO level as well as the largely blue-shifted absorption spectrum compared to the Y6 host acceptor. The upshifted LUMO level of Y-T leads to a higher $V_{oc}$ in the PM6:Y6:Y-T ternary system than that of the PM6:Y6 binary system. The largely blue-shifted absorption of Y-T well fills the absorption gap between PM6 and Y6, and the similarity between Y6 and Y-T acceptors in the core structure provides good compatibility in the active layer and reduces energetic disorders. By incorporating Y-T into the PM6:Y6 binary system, the champion ternary device yields an outstanding PCE of 17.37%, which is significantly higher than that of the binary PM6:Y6 device (15.64%). The improved PCE in the PM6:Y6:Y-T ternary device is attributed to the concurrently increased $V_{oc}$, $J_{sc}$ and FF. The energy loss of

the PM6:Y6:Y-T ternary OSC is also reduced to 0.455 eV. Further detailed characterizations reveal that the formation of alloy-like acceptor composite with very efficient energy transfer in the ternary blend. Moreover, the addition of weakly crystalline and edge-on orientated Y-T guest acceptor can reduce the strong aggregation tendency of Y6 and form the well-mixed three-dimension (3D) phase separation through a co-alloy phase, which is more favorable for vertical charge transport and depression of carrier recombination. These results offer a new perspective on the design of novel guest electron acceptors for higher performance ternary OSCs.

**2. Results and Discussion**

Y-T is synthesized by Knoevenagel condensation reaction between 12,13-bis(2-ethyl hexyl)-3,9-diundecyl-12,13-dihydro[1,2,5]thiadiazolo[3,4e]thieno[2″,3″:4′,5′]thieno [2hieno3,9-pyrrolo[3,2g]thieno[3,2-b]indole-2,10-dicarbaldehyde (S1) and 1,3-diethyl-2-thiobarbituric acid (DTBA). The synthetic details and characterizations of Y-T are provided in the Supporting Information. The target molecule Y-T can dissolve well in common organic solvents including dichloromethane, chloroform and chlorobenzene with solubility $>$ 10 mg/mL. The chemical structures of the host and guest electron acceptors (Y6 and Y-T), and the electron donor polymer PM6 are depicted in Fig. 1a. It is known that the charge transfer behavior between the DA'D core and the end-group A determines the optical characteristics in this A-DA'D-A type acceptor. Instead of the commonly used IC derivatives as the end group of Y6-series acceptors, the much weaker electron-withdrawing character of DTBA end group will

therefore be able to alter the optical and electronic properties pronouncedly. In chloroform solution, Y-T shows a blue-shifted absorption (~77 nm) with a maximum molar coefficient of $1.38 \times 10^5$ $M^{-1}$ $cm^{-1}$ (653 nm) relative to that of Y6, due to the electron-withdrawing effects of DTBA end group on the DA'D core (Fig. S1). From solution to film, the similar difference in absorption peaks are still observed for Y-T and Y6 films, respectively, as shown in Fig. 1b. More importantly, the absorption spectra of Y-T ranges from 500 to 730 nm with a medium bandgap of 1.64 eV, providing the possibility to make full use of the absorption gap in PM6:Y6 binary blend, which is favorable to enhance the solar energy utilization (Fig. 1b). Besides absorption complementarity, the addition of Y-T guest acceptor in PM6:Y6 blend may install a cascade energy transfer from Y-T to Y6 in the ternary system [44-46]. Fig. 1c shows the steady-state PL spectra of Y6, Y-T and Y6:Y-T blends with the weight ratios of 9:1 and 8:2 under excitation at 532 nm. The emission spectra of Y-T is ranged from 650 nm to 900 nm with the emission peak at 733 nm and has good overlap with the absorption spectra of Y6 (Fig. 1c), which fulfills the requirement for the fluorescence resonance energy transfer (FRET) from Y-T to Y6 [47]. When adding a small amount of Y-T into Y6, the emission of Y6 is gradually increased and blue-shifted with increasing fraction of Y-T. Also the emission from Y-T is completely quenched in the Y6:Y-T blend even at 10wt%, indicating that there is an efficient FRET, which provides an extra pathway for utilizing photo energy and may contributes to the enhanced photocurrent in ternary devices. In addition, this efficient FRET process suggests the good miscibility and compatibility in the Y6 and Y-T co-alloy phase.

As discussed above, a higher-lying LUMO level in the guest acceptor than that of the host acceptor may be able to increase the $V_{oc}$ in the ternary OSC, and it is known that the electron-withdrawing strength of the end group in NFA determines the LUMO level. Therefore, it is expected that Y-T has a higher-lying LUMO level than that of Y6 because of the much weaker electron-withdrawing strength of DTBA in Y-T than that of IC in Y6. As shown in Fig. 1d and Fig. S2, Y-T possesses a significantly raised LUMO level of -3.70 eV compared to Y6 (-4.10 eV). The highest occupied molecular orbital (HOMO) level of Y-T is estimated to be -5.42 eV, which showed an obvious HOMO mismatch in the driving force for exciton separation. However, in the ternary blend the two miscible acceptors with very similar molecular structures are considered to form a mixed phase and act as an alloyed acceptor, the energy level of which is closely associated with the $V_{oc}$ and exciton dissociation [29, 40, 42]. To verify this, the energy levels of Y6:Y-T blend films with different weight ratios are characterized using electrochemical methods. As shown in Fig. S2, the HOMO and LUMO levels of Y6:Y-T blend films show a linear change with respect to different Y-T weight ratios, implying that Y6 and Y-T formed an alloyed phase with a unified energy level [41].

The photovoltaic performance of the binary and ternary OSCs are investigated using a conventional device architecture of ITO/PEDOT:PSS/active layer/PFN-Br/Ag. All the devices are fabricated with a fixed donor/acceptor (D/A) weight ratio of 1:1.2, and the ternary OSCs are constructed by tuning the Y-T content (5 wt%, 10 wt% and 15 wt%) in the acceptor mixture. The detailed device fabrication is described in Supporting Information. The *J*-*V* curves of the optimal devices are shown in Fig. 2a

and the detailed photovoltaic parameters are provided in Table 1. The PM6:Y6 binary control device shows a PCE of 15.64% with a $V_{oc}$ of 0.846 V, a $J_{sc}$ of 26.37 mA/cm$^2$, and a fill factor (FF) of 70.30%, which is comparable with the reported values [10, 17, 43]. On the other hand, the binary OSC based on PM6 and Y-T exhibits a poor PCE of 5.06% and a remarkably high $V_{oc}$ of 1.19 V, resulting from the smaller energetic offset but mismatched HOMO levels between electron donor and acceptor. For ternary OSCs, adding 5 wt% of Y-T into the PM6:Y6 blend slightly increases the PCE to 16.28% and decreases the energy loss to 0.470 eV with simultaneous improvement of $V_{oc}$ and FF. The ternary device based on PM6:Y6:10 wt% Y-T blend shows a champion PCE as high as 17.37%, together with an enhanced $V_{oc}$ of 0.865 V, a slightly increased $J_{sc}$ of 26.90 mA/cm$^2$, and an improved FF of 74.97%. Further increasing Y-T ratio (15 wt%) will slightly decrease the PCE and energy loss, and the efficiency remained higher (17.11%) than that of the PM6:Y6 binary control device (15.64%). In addition, the near-linear compositional dependence of $V_{oc}$ is observed in Fig. 2b, confirming that Y6 and Y-T can form an electronic alloy acceptor and create an energy cascade. The PL spectra provides more information to understand the performance difference in the binary and ternary devices. As shown in Fig. S3 (Supporting Information), the emission of Y6 can be effectively quenched in the ternary blend, while PM6:Y6 binary film exhibits relatively higher PL intensity. The results demonstrate that introduction of Y-T can induce more efficient exciton dissociation and further explain the enhancement of $J_{sc}$, FF and PCE in the ternary device. In contrast, a strong PL emission of Y-T can be clearly observed in PM6:Y-T blend film,

indicating an unfavorable exciton dissociation and consistent with the mismatched energy levels as well as the poor device efficiency. We also listed in Fig. 2c the recently reported PM6:Y6-based representative ternary devices that incorporated a guest component [24-27, 35, 37, 40-42, 48-58]. It is notable that the ternary cells containing Y-T guest acceptor yielded simultaneously improved PCE and $V_{oc}$ without sacrificing $J_{sc}$, giving rise to a $J_{sc}$ of 26.90 mA/cm$^2$ which is the highest value reported so far for PM6:Y6-based ternary OSCs. This work shows that constructing ternary OSCs based on host-guest materials with very similar structures is a simple yet effective approach for further improving device performance.

The external quantum efficiency (EQE) spectra illustrated that both PM6:Y6 binary and ternary devices showed nearly identical responses from 300 to about 950 nm with over 80% EQE values (Fig. 2d). As shown in Fig. S4, we further investigated the EQE spectral difference (ΔEQE, calculated by $EQE_{ternary}$–$EQE_{binary}$), and found that the positive ΔEQE curve is covering from 300-570 and 670-820 nm, due to the enhanced spectral utilization and possibly optimized phase separation after the addition of Y-T. Besides, device based on PM6:Y-T blend exhibits a significantly lower and narrower response, which is consistent with the poor $J_{sc}$ value from *J*-*V* tests. Accordingly, the calculated $J_{sc}$ values integrated from the EQE spectra are 26.30, 8.97 and 26.43 mA/cm$^2$ for the Y6 binary, Y-T binary and ternary devices, respectively. To reveal the effect of guest acceptor on the charge recombination behavior, the dependence of $V_{oc}$ and $J_{sc}$ on the light intensity ($P_{light}$) have been measured. The slopes of the $V_{oc}$-$P_{light}$ curves help understand the degree of trap-assisted recombination, and

the undesirable recombination could be ignored when the slope is close to $kT/q$ [59]. As shown in Fig. 2e, the calculated slopes are 1.13 $kT/q$, 1.63 $kT/q$, and 1.02 $kT/q$ for PM6:Y6, PM6:Y-T, and the ternary devices, respectively, suggesting the significantly suppressed trap-assisted recombination in the optimal ternary devices. On the other hand, the dependence of $J_{sc}$ on the light intensity is also investigated by a power law equation $J_{sc} \propto P_{light}^{\alpha}$ [60]. Both binary devices show $\alpha$ values close to unit and the closest value can be observed in the ternary device, implying that the bimolecular recombination is further reduced after incorporation of guest acceptor Y-T. These results indicated that the PM6:Y6:Y-T ternary system exhibits effectively suppressed trap-assisted recombination and bimolecular recombination, which agreed well with higher $J_{sc}$ and FF. To understand the distinct improvement of FF value in ternary devices, hole and electron mobilities are evaluated by the space charge limited current (SCLC) method and the results are shown in Fig. S5 and Fig. 2f. Compared with PM6:Y-T device, PM6:Y6 binary and ternary devices exhibit higher charge carrier mobilities. Moreover, the Y6 binary device shows a slightly higher hole mobility than the ternary blend, while more balanced charge transport is observed in the ternary blend, consistent with the relatively high FF of 74.97% for the ternary devices.

The molecular packing and orientation properties of the neat and blend films are studied by grazing-incidence wide-angle X-ray scattering (GIWAXS). As shown in Fig. 3a, strong out-of-plane (OOP) π-π diffraction peaks are observed at 1.717 $Å^{-1}$ and 1.704 $Å^{-1}$ for Y6 and PM6 neat films, respectively, indicating good crystallinity and preferred face-on orientation, consistent with the reported results [16, 61, 62]. In

comparison with Y6, the pristine Y-T film shows a preferential edge-on orientation and a weak in-plane (IP) π-π diffraction peak was found at 1.609 $Å^{-1}$ with a *d*-spacing of 3.905 Å, suggesting that the crystallinity and molecular orientation of acceptors can be tuned by end group engineering [63]. The corresponding line-cut intensity profiles along the OOP and IP directions are described in Fig. 3b. Accordingly, Y-T in neat film shows a considerably lower crystalline coherence length (CCL) and peak area of π-π diffraction peak in OOP direction than that of neat Y6 (Fig. 3c, Fig. 3d and Table S1), further confirming the relatively weaker crystallization propensity of Y-T. Besides, the peak area ratios between OOP and IP directions are 6 and 10 for Y6 and PM6, respectively, while that of Y-T is 0.73, implying that the π-π stacking of Y-T may favor an edge-on orientation, as shown in Fig. S6. Fig. 3e plots the azimuthal angular distributions of the π-π stacking peaks. The Y-T film exhibits an apparent orientation distribution in small azimuthal angle range, while the neat Y6 and PM6 films exhibit a dominant peak at 90°, all consistent with their respective edge-on and face-on orientations with respect to the substrate.

2D GIWAXS and scattering profiles of the blend films are shown in Fig. 4, and these related parameters are summarized in Supporting Information (Table S2). As shown in Fig. 4a, both binary and ternary films adopt a face-on orientation with strong OOP π-π stacking peaks between 1.71 $Å^{-1}$ and 1.78 $Å^{-1}$, matching well with the azimuthal intensity profiles for the blend films (Fig. S7a). More specifically, PM6:Y6 binary film exhibits closer π-π stacking ($q_z$ = 1.783 $Å^{-1}$, *d*-spacing = 3.524 Å) and higher crystallinity (CCL = 18.23 Å) in the OOP direction than the PM6:Y-T binary

film ($q_z$ = 1.711 Å$^{-1}$, *d*-spacing = 3.673 Å, and CCL = 13.77 Å), suggesting that the molecular packing features of the neat films were preserved in the blends (Fig. 4b and Table S2).

For the ternary blend, the OOP π-π characteristic peak shifted to 1.744 Å00$^{-1}$ with a slightly lower CCL value of 18.07 Å when compared with the PM6:Y6 film (Fig. S7b), indicating that small ratio of Y-T does not perturb the crystallite orientation of PM6:Y6 blend, but slightly weaker crystallinity in the ternary film can be expected, which correlates well with marginally reduced but balanced charge mobility. Considering these diffractive features and the formation of electronic alloy phase as discussed above, we speculate that a small fraction of 3D acceptor alloy exist in the ternary film, which not only maintain the favorable face-on crystalline orientation with respect to the substrate, but also lead to the formation of three-dimensional phase separation and provide more charge transport channels, as shown in Fig. 4c. Such alloyed microstructure may be beneficial to facilitate charge transport and suppress carrier recombination, consistent with the enhancement of $J_{sc}$ and FF as well as PCE in ternary devices.

The morphologies of the binary and ternary active blends are further investigated by atomic force microscopy (AFM). As shown in Fig. 5, the PM6:Y6 and PM6:Y-T binary films display larger aggregates with a root-mean-square (RMS) surface roughness of 1.58 nm and 2.03 nm, respectively. It is clear that after adding 10 wt% Y-T, the morphology of ternary active layer is modified with a decreased RMS of 0.997 nm, implying that small amount of the guest acceptor plays a positive role in

optimizing surface morphology and phase separation. From the 3D height images, we can find that the ternary film shows smaller and more uniform film surface than the binary films, which improves exciton dissociation and is consistent with the GIWAXS results.

## 3. Conclusion

In summary, we have developed a new Y-series guest acceptor (Y-T) by employing weakly electron-withdrawing DTBA as the terminal group. Compared with the PM6:Y6 binary control device (15.64%), the optimal ternary device delivers an impressive PCE of 17.37% (11% enhancement), with simultaneous improvement of $V_{oc}$, $J_{sc}$, and FF. Systematic investigation of the role of Y-T as the third component in the ternary system reveals that the Y-T guest acceptor not only acts as energy-level and crystallization modulators, but also provides additional energy transfer channel and well-mixed 3D alloy acceptor phase in the ternary blend, which contribute synergistically to produce superior device performance. These results demonstrate that constructing guest molecules with similar structural backbone of host material is a promising strategy to further improve the PCE of state-of-the-art binary OSCs.

## Credit author contribution statement

**Yuli Yin:** synthesized the Y-T material and performed the NMR, GIWAXS and AFM experiment. **Lingling Zhan:** carried out the device fabrication and analyzed the data. **Ming Liu:** finished the CV measurements and analysis. **Chongqing Yang:** finished the $^{12}$CNMR and MALDI-TOF MS measurements and analysis. **Fengyun Guo:** conducted the UV measurements. **Yi Liu:** Supervision, conceived the idea, designed

the experiments and supervised the whole project. **Shiyong Gao:** performed the PL measurements; **Liancheng Zhao:** provided discussion and suggestions. **Hongzheng Chen:** Supervision, conceived the idea, designed the experiments and supervised the whole project. **Yong Zhang:** Supervision, conceived the idea, designed the experiments and supervised the whole project.

**Declaration of competing interest**

The authors declare no competing financial interest.

**Acknowledgements**

The authors acknowledge the support from the National Key Research and Development Program (2021YFE0105800 and 2019YFA0705900), the National Natural Science Foundation of China (22175049 and 21734008) and Natural Science Foundation of Heilongjiang Province of China (E2018036). We thank Dr. Xinle Li and Dr. Qin Hu for the assistance with GIWAXS measurements, and thank eceshi (www.eceshi.com) for the HR-MS analysis. Part of this work was carried out as a user project at the Molecular Foundry, and the GIWAXS characterization were performed at Advanced Light Source, Lawrence Berkeley National Laboratory, all supported by the Office of Science, Office of Basic Energy Sciences, of the U.S. Department of Energy under contract no. DE-AC02-05CH11231. Y. Zhang thanks the support from the Fundamental Research Funds for the Central Universities (Harbin Institute of Technology).

**Appendix A. Supporting information**

Supplementary data associated with this article can be found in the online version at

doi: ****.

## References

[1] Y. Lin, J. Wang, Z.G. Zhang, H. Bai, Y. Li, D. Zhu, X. Zhan, An electron acceptor challenging fullerenes for efficient polymer solar cells, Adv. Mater. 27 (2015) 1170-1174.
[2] S. Holliday, R.S. Ashraf, A. Wadsworth, D. Baran, S.A. Yousaf, C.B. Nielsen, C.H. Tan, S.D. Dimitrov, Z. Shang, N. Gasparini, M. Alamoudi, F. Laquai, C.J. Brabec, A. Salleo, J.R. Durrant, I. McCulloch, High-efficiency and air-stable P3HT-based polymer solar cells with a new non-fullerene acceptor, Nat. Commun. 7 (2016) 11585.
[3] Z. Xiao, X. Jia, D. Li, S. Wang, X. Geng, F. Liu, J. Chen, S. Yang, T.P. Russell, L. Ding, 26 mA cm$^{-2}$ $J_{sc}$ from organic solar cells with a low-bandgap nonfullerene acceptor, Sci. Bull. 62 (2017) 1494-1496.
[4] W. Zhao, S. Li, H. Yao, S. Zhang, Y. Zhang, B. Yang, J. Hou, Molecular optimization enables over 13% efficiency in organic solar cells, J. Am. Chem. Soc. 139 (2017) 7148-7151.
[5] S. Li, L. Zhan, F. Liu, J. Ren, M. Shi, C.Z. Li, T.P. Russell, H. Chen, An unfused-core-based nonfullerene acceptor enables high-efficiency organic solar cells with excellent morphological stability at high temperatures, Adv. Mater. 30 (2018) 1705208.
[6] L. Meng, Y. Zhang, X. Wan, C. Li, X. Zhang, Y. Wang, X. Ke, Z. Xiao, L. Ding, R. Xia, H.L. Yip, Y. Cao, Y. Chen, Organic and solution-processed tandem solar cells with 17.3% efficiency, Science 361 (2018) 1094-1098.
[7] B. He, B. Yang, M.A. Kolaczkowski, C.A. Anderson, L.M. Klivansky, T.L. Chen, M.A. Brady, Y. Liu, Molecular engineering for large open-circuit voltage and low energy loss in around 10% non-fullerene organic photovoltaics, ACS Energy Lett. 3 (2018) 1028-1035.
[8] Y. Yin, Z. Zheng, D. Chen, M. Liu, J. Zhang, F. Guo, S. Gao, L. Zhao, Y. Zhang, Fusion or non-fusion of quasi-two-dimensional fused perylene diimide acceptors: the importance of molecular geometry for fullerene-free organic solar cells, J. Mater. Chem. A, 7 (2019) 27493-27502.
[9] T. Li, Y. Wu, J. Zhou, M. Li, J. Wu, Q. Hu, B. Jia, X. Pan, M. Zhang, Z. Tang, Z. Xie, T.P. Russell, X. Zhan, Butterfly effects arising from starting materials in fused-ring electron acceptors, J. Am. Chem. Soc. 142 (2020) 20124-20133.
[10] J. Yuan, Y. Zhang, L. Zhou, G. Zhang, H.-L. Yip, T.-K. Lau, X. Lu, C. Zhu, H. Peng, P.A. Johnson, M. Leclerc, Y. Cao, J. Ulanski, Y. Li, Y. Zou, Single-junction organic solar cell with over 15% efficiency using fused-ring acceptor with electron-deficient core, Joule 3 (2019) 1140-1151.
[11] R. Ma, T. Liu, Z. Luo, Q. Guo, Y. Xiao, Y. Chen, X. Li, S. Luo, X. Lu, M. Zhang, Y. Li, H. Yan, Improving open-circuit voltage by a chlorinated polymer donor endows binary organic solar cells efficiencies over 17%, Sci. China Chem. 63 (2020) 325-330.

[12] F. Pan, C. Sun, Y. Li, D. Tang, Y. Zou, X. Li, S. Bai, X. Wei, M. Lv, X. Chen, Y. Li, Solution-processable n-doped graphene-containing cathode interfacial materials for high-performance organic solar cells, Energy Environ. Sci. 12 (2019) 3400-3411.
[13] Q. Yang, S. Yu, P. Fu, W. Yu, Y. Liu, X. Liu, Z. Feng, X. Guo, C. Li, Boosting performance of non-fullerene organic solar cells by 2D g-$C_3N_4$ doped PEDOT:PSS, Adv. Funct. Mater. 30 (2020) 1910205.
[14] Q. Liu, Y. Jiang, K. Jin, J. Qin, J. Xu, W. Li, J. Xiong, J. Liu, Z. Xiao, K. Sun, S. Yang, X. Zhang, L. Ding, 18% Efficiency organic solar cells, Sci. Bull. 65 (2020) 272-275.
[15] C. Sun, F. Pan, S. Chen, R. Wang, R. Sun, Z. Shang, B. Qiu, J. Min, M. Lv, L. Meng, C. Zhang, M. Xiao, C. Yang, Y. Li, Achieving fast charge separation and low nonradiative recombination loss by rational fluorination for high-efficiency polymer solar cells, Adv. Mater. 31 (2019) 1905480.
[16] L. Zhu, M. Zhang, G. Zhou, T. Hao, J. Xu, J. Wang, C. Qiu, N. Prine, J. Ali, W. Feng, X. Gu, Z. Ma, Z. Tang, H. Zhu, L. Ying, Y. Zhang, F. Liu, Efficient organic solar cell with 16.88% efficiency enabled by refined acceptor crystallization and morphology with improved charge transfer and transport properties, Adv. Energy Mater. 10 (2020) 1904234.
[17] K. Jiang, Q. Wei, J.Y.L. Lai, Z. Peng, H.K. Kim, J. Yuan, L. Ye, H. Ade, Y. Zou, H. Yan, Alkyl chain tuning of small molecule acceptors for efficient organic solar cells, Joule 3 (2019) 3020-3033.
[18] X. Li, I. Angunawela, Y. Chang, J. Zhou, H. Huang, L. Zhong, A. Liebman-Pelaez, C. Zhu, L. Meng, Z. Xie, H. Ade, H. Yan, Y. Li, Effect of the chlorine substitution position of the end-group on intermolecular interactions and photovoltaic performance of small molecule acceptors, Energy Environ. Sci. 13 (2020) 5028-5038.
[19] Y. Cui, H. Yao, J. Zhang, K. Xian, T. Zhang, L. Hong, Y. Wang, Y. Xu, K. Ma, C. An, C. He, Z. Wei, F. Gao, J. Hou, Single-junction organic photovoltaic cells with approaching 18% efficiency, Adv. Mater. (2020) 1908205.
[20] Z. Zhou, W. Liu, G. Zhou, M. Zhang, D. Qian, J. Zhang, S. Chen, S. Xu, C. Yang, F. Gao, H. Zhu, F. Liu, X. Zhu, Subtle molecular tailoring induces significant morphology optimization enabling over 16% efficiency organic solar cells with efficient charge generation, Adv. Mater. 32 (2020) 1906324.
[21] Q. Wei, W. Liu, M. Leclerc, J. Yuan, H. Chen, Y. Zou, A-DA′D-A non-fullerene acceptors for high-performance organic solar cells, Sci. China Chem. 63 (2020) 1352-1366.
[22] F. Qi, K. Jiang, F. Lin, Z. Wu, H. Zhang, W. Gao, Y. Li, Z. Cai, H.Y. Woo, Z. Zhu, A.K.Y. Jen, Over 17% efficiency binary organic solar cells with photoresponses reaching 1000 nm enabled by selenophene-fused nonfullerene acceptors, ACS Energy Lett. 6 (2021) 9-15.
[23] Z. Zhang, Y. Li, G. Cai, Y. Zhang, X. Lu, Y. Lin, Selenium heterocyclic electron acceptor with small urbach energy for as-cast high-performance organic solar cells, J. Am. Chem. Soc. 142 (2020) 18741-18745.

[24] R. Ma, T. Liu, Z. Luo, K. Gao, K. Chen, G. Zhang, W. Gao, Y. Xiao, T.-K. Lau, Q. Fan, Y. Chen, L.-K. Ma, H. Sun, G. Cai, T. Yang, X. Lu, E. Wang, C. Yang, A.K.Y. Jen, H. Yan, Adding a third component with reduced miscibility and higher LUMO level enables efficient ternary organic solar cells, ACS Energy Lett. 5 (2020) 2711-2720.
[25] D. Li, L. Zhu, X. Liu, W. Xiao, J. Yang, R. Ma, L. Ding, F. Liu, C. Duan, M. Fahlman, Q. Bao, Enhanced and balanced charge transport boosting ternary solar cells over 17% efficiency, Adv. Mater. 32 (2020) 2002344.
[26] N. Gasparini, S.H.K. Paleti, J. Bertrandie, G. Cai, G. Zhang, A. Wadsworth, X. Lu, H.-L. Yip, I. McCulloch, D. Baran, Exploiting ternary blends for improved photostability in high-efficiency organic solar cells, ACS Energy Lett. 5 (2020) 1371-1379.
[27] Q. An, J. Wang, W. Gao, X. Ma, Z. Hu, J. Gao, C. Xu, M. Hao, X. Zhang, C. Yang, F. Zhang, Alloy-like ternary polymer solar cells with over 17.2% efficiency, Sci. Bull. 65 (2020) 538-545.
[28] X. Ma, A. Zeng, J. Gao, Z. Hu, C. Xu, J. Son, S. Jeong, C. Zhang, M. Li, K. Wang, H. Yan, Z. Ma, Y. Wang, H. Woo, F. Zhang, Approaching 18% efficiency of ternary organic photovoltaics with wide bandgap polymer donor and well compatible Y6 : Y6-1O as acceptor, Natl. Sci. Rev. 8 (2021) nwaa305.
[29] Y. Zhang, G. Li, Functional third components in nonfullerene acceptor-based ternary organic solar cells, Acc. Mater. Res. 1 (2020) 158-171.
[30] N. Gasparini, A. Salleo, I. McCulloch, D. Baran, The role of the third component in ternary organic solar cells, Nat. Rev. Mater. 4 (2019) 229-242.
[31] Q. An, F. Zhang, J. Zhang, W. Tang, Z. Deng, B. Hu, Versatile ternary organic solar cells: a critical review, Energy Environ. Sci. 9 (2016) 281-322.
[32] X. Xu, K. Feng, Y.W. Lee, H.Y. Woo, G. Zhang, Q. Peng, Subtle polymer donor and molecular acceptor design enable efficient polymer solar cells with a very small energy loss, Adv. Funct. Mater. 30 (2020) 1907570.
[33] H. Lu, J. Zhang, J. Chen, Q. Liu, X. Gong, S. Feng, X. Xu, W. Ma, Z. Bo, Ternary-blend polymer solar cells combining fullerene and nonfullerene acceptors to synergistically boost the photovoltaic performance, Adv. Mater. 28 (2016) 9559-9566.
[34] Z. Zhou, S. Xu, J. Song, Y. Jin, Q. Yue, Y. Qian, F. Liu, F. Zhang, X. Zhu, High-efficiency small-molecule ternary solar cells with a hierarchical morphology enabled by synergizing fullerene and non-fullerene acceptors, Nat. Energy 3 (2018) 952-959.
[35] R. Yu, H. Yao, Y. Cui, L. Hong, C. He, J. Hou, Improved charge transport and reduced nonradiative energy loss enable over 16% efficiency in ternary polymer solar cells, Adv. Mater. 31 (2019) 1902302.
[36] T. Liu, Z. Luo, Y. Chen, T. Yang, Y. Xiao, G. Zhang, R. Ma, X. Lu, C. Zhan, M. Zhang, C. Yang, Y. Li, J. Yao, H. Yan, A nonfullerene acceptor with a 1000 nm absorption edge enables ternary organic solar cells with improved optical and morphological properties and efficiencies over 15%, Energy Environ. Sci. 12 (2019) 2529-2536.
[37] K. Li, Y. Wu, Y. Tang, M.-A. Pan, W. Ma, H. Fu, C. Zhan, J. Yao, Ternary blended

fullerene-free polymer solar cells with 16.5% efficiency enabled with a higher-LUMO-level acceptor to improve film morphology, Adv. Energy Mater. (2019) 1901728.
[38] L. Xiao, B. He, Q. Hu, L. Maserati, Y. Zhao, B. Yang, M.A. Kolaczkowski, C.L. Anderson, N.J. Borys, L.M. Klivansky, T.L. Chen, A.M. Schwartzberg, T.P. Russell, Y. Cao, X. Peng, Y. Liu, Multiple roles of a non-fullerene acceptor contribute synergistically for high-efficiency ternary organic photovoltaics, Joule 2 (2018) 2154.
[39] M. Zhang, W. Gao, F. Zhang, Y. Mi, W. Wang, Q. An, J. Wang, X. Ma, J. Miao, Z. Hu, X. Liu, J. Zhang, C. Yang, Efficient ternary non-fullerene polymer solar cells with PCE of 11.92% and FF of 76.5%, Energy Environ. Sci. 11 (2018) 841-849.
[40] L. Zhan, S. Li, T.-K. Lau, Y. Cui, X. Lu, M. Shi, C.-Z. Li, H. Li, J. Hou, H. Chen, Over 17% efficiency ternary organic solar cells enabled by two non-fullerene acceptors working in an alloy-like model, Energy Environ. Sci. 13 (2020) 635-645.
[41] S. Li, L. Zhan, Y. Jin, G. Zhou, T.K. Lau, R. Qin, M. Shi, C.Z. Li, H. Zhu, X. Lu, F. Zhang, H. Chen, Asymmetric electron acceptors for high-efficiency and low-energy-loss organic photovoltaics, Adv. Mater. 32 (2020) 2001160.
[42] T. Liu, R. Ma, Z. Luo, Y. Guo, G. Zhang, Y. Xiao, T. Yang, Y. Chen, G. Li, Y. Yi, X. Lu, H. Yan, B. Tang, Concurrent improvement in $J_{sc}$ and $V_{oc}$ in high-efficiency ternary organic solar cells enabled by a red-absorbing small-molecule acceptor with a high LUMO level, Energy Environ. Sci. 13 (2020) 2115-2123.
[43] Y. Zhang, G. Cai, Y. Li, Z. Zhang, T. Li, X. Zuo, X. Lu, Y. Lin, An electron acceptor analogue for lowering trap density in organic solar cells, Adv. Mater. 33 (2021) 2008134.
[44] A.R. Clapp, I.L. Medintz, J.M. Mauro, B.R. Fisher, M.G. Bawendi, H. Mattoussi, Fluorescence resonance energy transfer between quantum dot donors and dye-labeled protein acceptors, J. Am. Chem. Soc. 126 (2004) 301-310.
[45] L. Nian, K. Gao, F. Liu, Y. Kan, X. Jiang, L. Liu, Z. Xie, X. Peng, T.P. Russell, Y. Ma, 11% Efficient ternary organic solar cells with high composition tolerance via integrated near-IR sensitization and interface engineering, Adv. Mater. 28 (2016) 8184-8190.
[46] W. Li, Y. Yan, Y. Gong, J. Cai, F. Cai, R.S. Gurney, D. Liu, A.J. Pearson, D.G. Lidzey, T. Wang, Contrasting effects of energy transfer in determining efficiency improvements in ternary polymer solar cells, Adv. Funct. Mater. 28 (2018) 1704212.
[47] K.E. Sapsford, L. Berti, I.L. Medintz, Materials for fluorescence resonance energy transfer analysis: beyond traditional donor-acceptor combinations, Angew. Chem. Int. Ed. 45 (2006) 4562-4589.
[48] T. Yan, J. Ge, T. Lei, W. Zhang, W. Song, B. Fanady, D. Zhang, S. Chen, R. Peng, Z. Ge, 16.55% efficiency ternary organic solar cells enabled by incorporating a small molecular donor, J. Mater. Chem. A, 7 (2019) 25894-25899.
[49] X. Chen, Q. Zhang, D. Wang, X. Xu, Z. Wang, Y. Li, H. Zhu, X. Lu, W. Chen, H. Qiu, C.-Z. Li, High-efficiency ternary organic solar cells based on the synergized polymeric and small-molecule donors, Solar RRL 4 (2020) 2000537.

[50] J. Han, X. Wang, D. Huang, C. Yang, R. Yang, X. Bao, Employing asymmetrical thieno[3,4-d]pyridazin-1(2H)-one block enables efficient ternary polymer solar cells with improved light-harvesting and morphological properties, Macromolecules 53 (2020) 6619-6629.
[51] Q. An, J. Wang, X. Ma, J. Gao, Z. Hu, B. Liu, H. Sun, X. Guo, X. Zhang, F. Zhang, Two compatible polymer donors contribute synergistically for ternary organic solar cells with 17.53% efficiency, Energy Environ. Sci. 13 (2020) 5039-5047.
[52] J. Song, C. Li, L. Zhu, J. Guo, J. Xu, X. Zhang, K. Weng, K. Zhang, J. Min, X. Hao, Y. Zhang, F. Liu, Y. Sun, Ternary organic solar cells with efficiency >16.5% based on two compatible nonfullerene acceptors, Adv. Mater. 31 (2019) 1905645.
[53] Y. Qin, H. Chen, J. Yao, Y. Zhou, Y. Cho, Y. Zhu, B. Qiu, C.W. Ju, Z.G. Zhang, F. He, C. Yang, Y. Li, D. Zhao, Silicon and oxygen synergistic effects for the discovery of new high-performance nonfullerene acceptors, Nat. Commun. 11 (2020) 5814.
[54] C. Yan, R. Ma, G. Cai, T. Liu, J. Zhu, J. Wang, Y. Li, J. Huang, Z. Luo, Y. Xiao, X. Lu, T. Yang, X. Zhan, H. Yan, G. Li, Reducing $V_{oc}$ loss via structure compatible and high lowest unoccupied molecular orbital nonfullerene acceptors for over 17%-efficiency ternary organic photovoltaics, EcoMat 2 (2020) e12061.
[55] Q. Ma, Z. Jia, L. Meng, J. Zhang, H. Zhang, W. Huang, J. Yuan, F. Gao, Y. Wan, Z. Zhang, Y. Li, Promoting charge separation resulting in ternary organic solar cells efficiency over 17.5%, Nano Energy 78 (2020) 105272.
[56] T. Yan, W. Song, J. Huang, R. Peng, L. Huang, Z. Ge, 16.67% rigid and 14.06% flexible organic solar cells enabled by ternary heterojunction strategy, Adv. Mater. 31 (2019) 1902210.
[57] X. Du, Y. Yuan, L. Zhou, H. Lin, C. Zheng, J. Luo, Z. Chen, S. Tao, L.S. Liao, Delayed fluorescence emitter enables near 17% efficiency ternary organic solar cells with enhanced storage stability and reduced recombination energy loss, Adv. Funct. Mater. 30 (2020) 1909837.
[58] M.-Y. Ni, S.-F. Leng, H. Liu, Y.-K. Yang, Q.-H. Li, C.-Q. Sheng, X. Lu, F. Liu, J.-H. Wan, Ternary organic solar cells with 16.88% efficiency enabled by a twisted perylene diimide derivative to enhance the open-circuit voltage, J. Mater. Chem. C 9 (2021) 3826-3834.
[59] Y. Yin, W. Zhang, Z. Zheng, Z. Ge, Y. Liu, F. Guo, S. Gao, L. Zhao, Y. Zhang, Integrated linker-regulation and ring-fusion engineering for efficient additive-free non-fullerene organic solar cells, J. Mater. Chem. C 8 (2020) 12516-12526.
[60] G.J. Zhang, G.F. Yang, H. Yan, J.H. Kim, H. Ade, W.L. Wu, X.P. Xu, Y.W. Duan, Q. Peng, Efficient nonfullerene polymer solar cells enabled by a novel wide bandgap small molecular acceptor, Adv. Mater. 29 (2017) 1606054.
[61] T. Liu, Z. Luo, Q. Fan, G. Zhang, L. Zhang, W. Gao, X. Guo, W. Ma, M. Zhang, C. Yang, Y. Li, H. Yan, Use of two structurally similar small molecular acceptors enabling ternary organic solar cells with high efficiencies and fill factors, Energy Environ. Sci. 11 (2018) 3275-3282.
[62] H. Fu, W. Gao, Y. Li, F. Lin, X. Wu, J.H. Son, J. Luo, H.Y. Woo, Z. Zhu, A.K.Y. Jen, A generally applicable approach using sequential deposition to enable highly efficient organic solar cells, Small Methods 4 (2020) 2000687.

[63] L. Xiao, M.A. Kolaczkowski, Y. Min, Y. Liu, Substitution effect on thiobarbituric acid end groups for high open-circuit voltage non-fullerene organic solar cells, ACS Appl. Mater. Interfaces 12 (2020) 41852-41860.

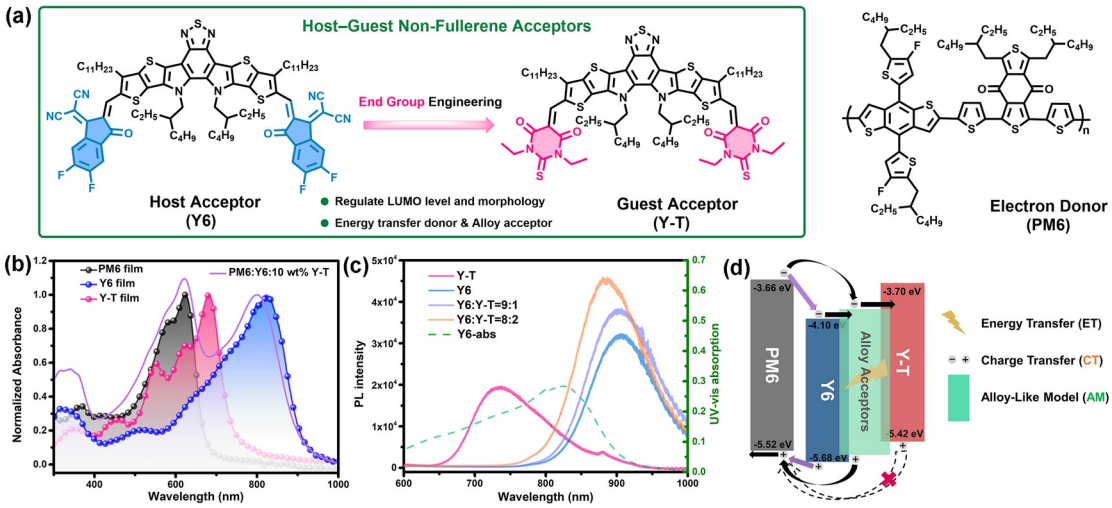


**Fig. 1.** a) Molecular structure of the host-guest non-fullerene acceptors (Y6 and Y-T) and the electron donor PM6. b) Normalized UV-Vis absorption spectra of the neat and ternary blend films. c) PL spectra of Y6, Y-T and their mixtures at the weight ratios of 9:1 and 8:2 under excitation at 532 nm. d) Schematics of the energy level and the working mechanism in this ternary OSCs.

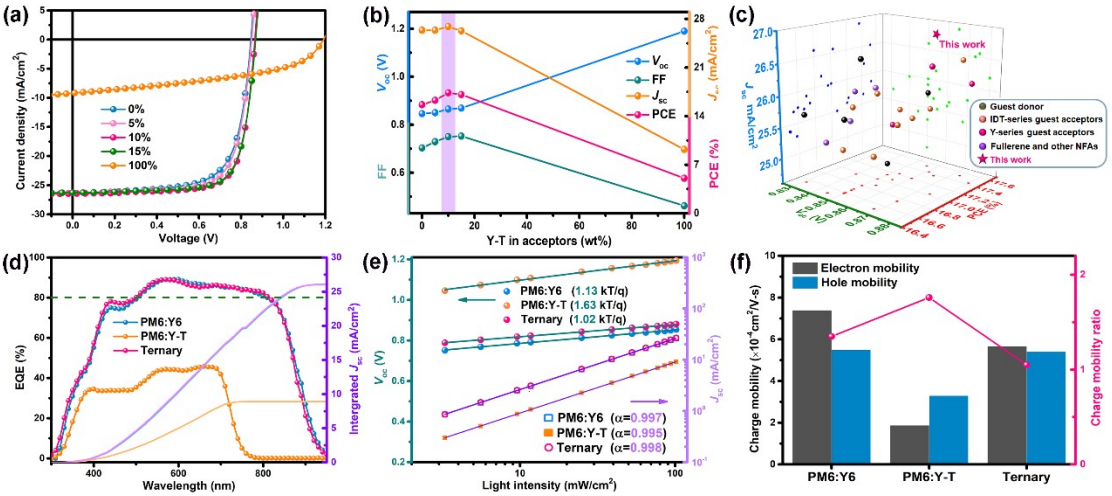


**Fig. 2.** a) *J-V* curves of the PM6:Y6-based OSCs with different weight ratios of Y-T. b) $V_{oc}$, $J_{sc}$, FF and PCE dependence on Y-T content in acceptors. c) Plots of $J_{sc}$ against $V_{oc}$ and PCE for PM6:Y6-based representative ternary devices in the literatures and in this study. d) EQE spectra of the binary and the optimal ternary devices. e) Plots of $V_{oc}$ and $J_{sc}$ against the incident light intensity ($P_{light}$) for the binary and the optimal ternary devices. f) Electron and hole mobilities and their ratios of the binary and the optimal ternary devices.

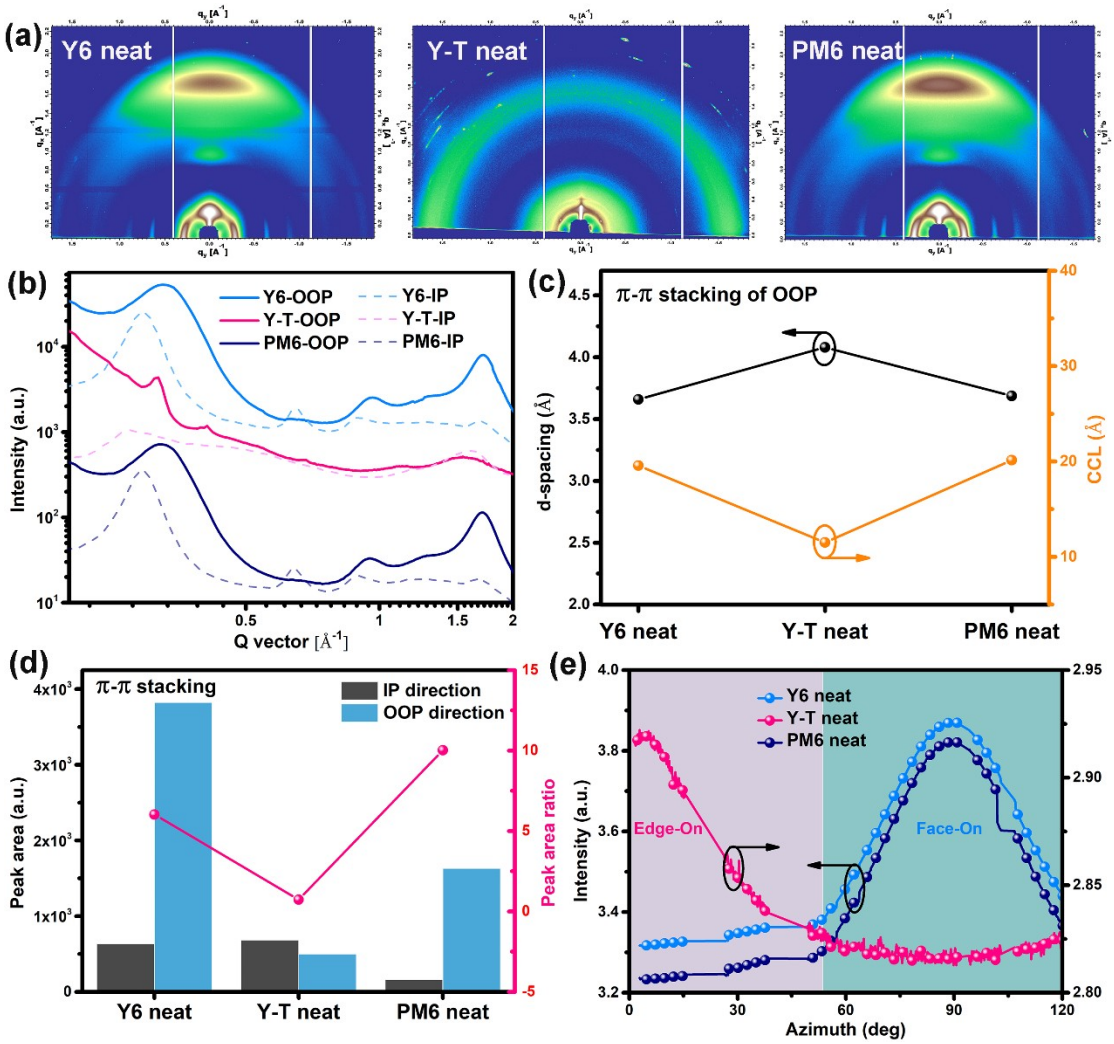


**Fig. 3.** a) 2D GIWAXS patterns for Y6, Y-T and PM6 neat films. b) Scattering profiles for Y6, Y-T and PM6 neat films. c) The *d*-spacing and crystal coherence length (CCL) of (010) diffraction planes in OOP direction for Y6, Y-T and PM6 neat films. d) The peak area and peak area ratio of (010) diffraction planes for Y6, Y-T and PM6 neat films. e) Azimuthal intensity profiles for Y6, Y-T and PM6 neat films.

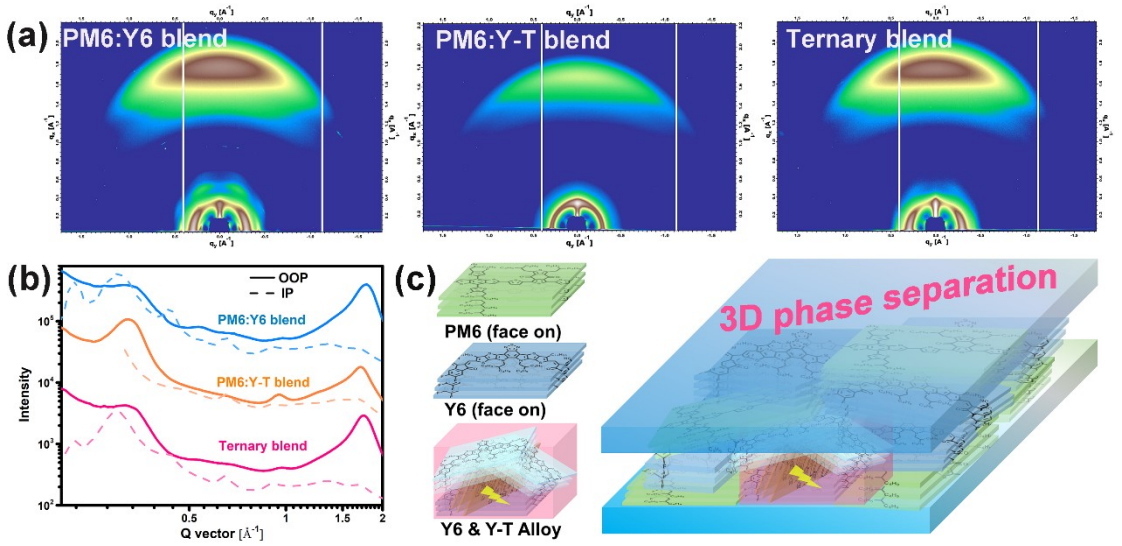


**Fig. 4.** a) 2D GIWAXS patterns for binary and ternary blend films. b) Scattering profiles for binary and ternary blend films. c) Molecular packing sketch map for the ternary film.

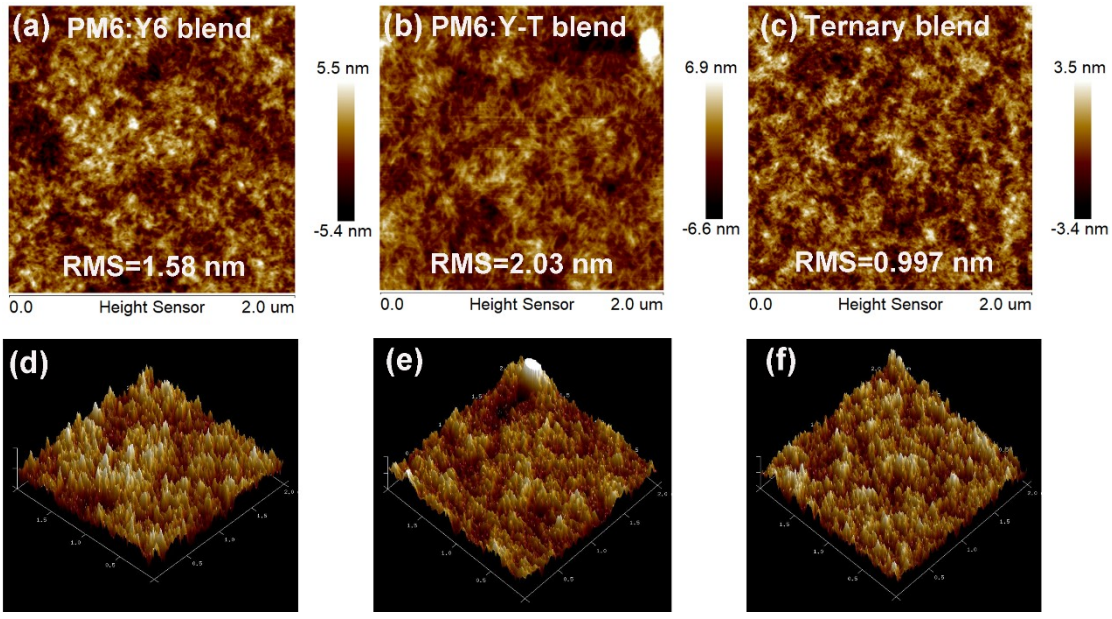


**Fig. 5.** AFM height and three-dimensional height images for binary and ternary blend films.

**Table 1.** Photovoltaic parameters of the ternary OSCs based on PM6:Y6:Y-T blends with various Y-T ratios

| Y-T ratio[a)] (wt %) | $V_{oc}$ (V) | $J_{sc}$ (mA/cm$^2$) | FF (%) | PCE[b)] (%) | $J_{cal}$[c)] (mA/cm$^2$) | $E_{loss}$[d)] (eV) |
|---|---|---|---|---|---|---|
| 0% | 0.846 | 26.37 | 70.30 | 15.64 (15.43 ± 0.18) | 26.30 | 0.474 |
| 5% | 0.850 | 26.37 | 72.88 | 16.28 (15.86 ± 0.25) | - | 0.470 |
| 10% | 0.865 | 26.90 | 74.97 | 17.37 (17.04 ± 0.21) | 26.43 | 0.455 |
| 15% | 0.869 | 26.28 | 75.24 | 17.11 (16.88 ± 0.20) | - | 0.451 |
| 100% | 1.190 | 9.21 | 46.15 | 5.06 (4.90 ± 0.12) | 8.97 | 0.450 |

[a)] Weight ratio of Y-T in the host-guest acceptor mixture (total D/A ratio is kept as 1:1.2); b) Values in parentheses are the average PCEs for ten devices; c) Calculated $J_{sc}$ from EQE curves; d) Energy loss calculated from the optical band gap of blend films and $V_{oc}$.